Rare Metal Materials and Engineering
Volume 54, Issue 8, August 2025
Available online at www.rmme.ac.cn

Science Press

Cite this article as: Xie Jing, Zhang Qian, Ren Jing, et al. Effects of Zr_2Cu Packing Modification on Microstructure and Mechanical and Ablation Properties of PIP-Prepared C/C-SiC-ZrC Composites[J]. Rare Metal Materials and Engineering, 2025, 54(08): 1940-1946. DOI: https://doi.org/10.12442/j.issn.1002-185X.20240401.

ARTICLE

Effects of Zr_2Cu Packing Modification on Microstructure and Mechanical and Ablation Properties of PIP-Prepared C/C-SiC-ZrC Composites

Xie Jing[1], Zhang Qian[1], Ren Jing[1], Su Hailong[2], Tian Lulu[2], Zhi Xionghui[2], Sun Guodong[1], Li Hui[1], Wang Long[3]

[1] School of Materials Science & Engineering, Chang'an University, Xi'an 710061, China; [2] Xi'an Xin Yao Ceramic Composite Materials Co., Ltd, Xi'an 710089, China; [3] Zhijian Laboratory, Rocket Force University of Engineering, Xi'an 710025, China

Abstract: To improve the compactness and properties of C/C-SiC-ZrC composites produced by precursor infiltration and pyrolysis (PIP) method, the low-temperature reactive melt infiltration (RMI) process was used to seal the composites using Zr_2Cu as the filler. The microstructure, mechanical properties, and ablation properties of the Zr_2Cu packed composites were analyzed. Results show that during Zr_2Cu impregnation, the melt efficiently fills the large pores of the composites and is converted to ZrCu due to a partial reaction of zirconium with carbon. This results in an increase in composite density from 1.91 g/cm^3 to 2.24 g/cm^3 and a reduction in open porosity by 27.35%. Additionally, the flexural strength of Zr_2Cu packed C/C-SiC-ZrC composites is improved from 122.78±8.09 MPa to 135.53±5.40 MPa. After plasma ablation for 20 s, the modified composites demonstrate superior ablative resistance compared to PIP C/C-SiC-ZrC, with mass ablation and linear ablation rates of 2.77×10^{-3} g/s and 2.60×10^{-3} mm/s, respectively. The "self-transpiration" effect of the low-melting point copper-containing phase absorbs the heat of the plasma flame, further reducing the ablation temperature and promoting the formation of refined ZrO_2 particles within the SiO_2 melting layer. This provides more stable erosion protection for Zr_2Cu packed C/C-SiC-ZrC composites.

Key words: C/C-SiC-ZrC composites; Zr_2Cu packing; microstructure; mechanical property; ablation property

1 Introduction

Carbon/carbon (C/C) composites have low density, high specific strength, low coefficient of thermal expansion, excellent high-temperature stability, and fine thermal shock resistance. They maintain structural strength above 3000 ℃, making them suitable for manufacturing solid rocket motor nozzles, throat liners, missile nose cones, and other high-temperature applications[1–3]. Unfortunately, C/C composites are prone to oxidation at temperatures above 400 °C, and the oxidation rate increases rapidly with temperature. This reduces their durability and performance, severely restricting their reliability as structural materials at high temperatures[4]. Improving the oxidation and ablation resistance of C/C composites under harsh conditions has become an urgent research focus. Introducing ultra-high temperature ceramics (UHTCs) has proven effective[5–7]. ZrC, a representative UHTC, has a high melting point, remarkable oxidation resistance, and commendable chemical stability. It is worth noting that the resulting oxidized product, ZrO_2, has an exceptionally high melting point of 2770 ℃. The generation of a shielding ZrO_2 film during the oxidation process can withstand external corrosive airflow, thereby enhancing the oxidation and ablation resistance of ZrC modified C/C composites[4,8–9]. However, ZrO_2 alone is relatively loose, so SiC and ZrC are often paired to modify C/C composites synergistically. SiO_2 has good mobility to seal cracks by

Received date: July 04, 2024
Foundation item: Open Fund of Zhijian Laboratory, Rocket Force University of Engineering (2024-ZJSYS-KF02-09); National Natural Science Foundation of China (51902028, 52272034); Key Research and Development Program of Shaanxi (2023JBGS-15); Fundamental Research Funds for the Central Universities (Chang'an University, 300102313202, 300102312406)
Corresponding author: Xie Jing, Ph. D., Associate Professor, School of Materials Science & Engineering, Chang'an University, Xi'an 710061, P. R. China, Tel: 0086-29-82337340, E-mail: xiejing@chd.edu.cn

filling the porous ZrO_2 framework, forming a dense continuous ZrO_2-SiO_2 protective layer[10–12].

Up to now, various approaches, such as chemical vapor infiltration (CVI) [13], reactive melt infiltration (RMI) [14–17], precursor infiltration, and pyrolysis (PIP) [18–21], have been employed to produce C/C-UHTCs composites. PIP is widely used due to its advantages in low-temperature forming, low fiber damage, good material composition designability, and the ability to produce complex molded parts[22–25]. However, the long preparation period due to repeated infiltration-pyrolysis cycles and lack of densification caused by high shrinkage during the precursor pyrolysis process degrades the properties of C/C-UHTCs composites[2]. Therefore, shortening the PIP process and improving the density of the pyrolytic matrix are essential in ablation resistance research.

To address these issues, new precursors with high ceramic yields have been synthesized and applied to improve the impregnation efficiency of PIP[26]. Combining multiple processes, especially PIP and RMI, has also been proposed in Ref.[27]. Liu et al[28] studied the C/C-ZrC-SiC surface with a uniformly distributed ZrC-SiC hybrid ceramic coating using PIP-RMI-PIP. Kong et al[29] prepared low-density C/C composites for melt infiltration by PIP, using $Si_{0.9}Zr_{0.1}$ alloy as the melt infiltration metal. They shortened the preparation cycle by using RMI to obtain C/C-ZrC-SiC composites with a density of 2.39 g/cm^3 and a flexural strength of 260 MPa. Zhao et al[17,30] prepared C/C-ZrC-SiC-ZrB_2 composites by combining B_4C-phenolic resin slurry infiltration with RMI of $ZrSi_2$, with the melting infiltration temperature reaching 2100 ℃. Currently, Zr/Si mixed powder or ZrSi alloys with high melting points are mainly used as infiltrators for preparing C/C-SiC-ZrC composites by RMI, resulting in relatively high preparation temperatures and potential erosion of carbon fibers.

ZrCu alloy has a low melting point (1000 – 1200 ℃), indicating a lower impregnation temperature and less fiber destruction[31]. In addition, the “heat sink” and “transpirational cooling” effects of Cu can reduce the ablation temperature and improve the ablation properties of the composites[32]. Currently, ZrCu alloy is mainly used for preparing C/C-ZrC-Cu composites[6,33], while ZrCu modified C/C-SiC-ZrC composites fabricated by combining PIP and RMI have seldom been described.

In the current study, with the purpose of reducing the preparation temperature and improving the density of the matrix, C/C-SiC-ZrC composites were firstly fabricated using PIP and then Zr_2Cu infiltration was performed using RMI since Zr_2Cu is a typical ZrCu alloy with a melting point of 1025 °C. The effects of introducing Zr_2Cu on the microstructure, mechanical properties, and ablation properties of the composites were analyzed. The corresponding ablation mechanism was proposed.

2 Experiment

Fig.1 shows a schematic diagram of the preparation process for Zr_2Cu packing modified C/C-SiC-ZrC composites. Initially, 2.5D needled carbon fiber felts, obtained from Yixing Tianniao High Technology Co., Ltd, Jiangsu, China, with a density of 0.45 g/cm^3, underwent densification via CVI. This process yielded porous C/C preforms with a density of 0.90 g/cm^3. A mixture comprising polycarbosilane sourced from the National University of Defense Technology, Changsha, China, and zirconium-containing polymer obtained from the Institute of Process Engineering, Chinese Academy of Sciences, Beijing, China, in a mass ratio of 4: 1, was dispersed in xylene to form a homogeneous solution, which served as the SiC-ZrC precursor. Subsequently, C/C-SiC-ZrC composites, designated as CSiZr, were produced through 12 cycles of infiltration-drying-heat treatment. The CSiZr composites were embedded in Zr_2Cu powder (Eno High-Tech Materials Development Co., Ltd, Qinhuangdao, Hebei, China) within a graphite crucible and then heat-treated under a pressure of 500 Pa. The RMI process was conducted at 1200 °C for 2 h to fully melt and to infiltrate the Zr_2Cu powder, followed by natural cooling to obtain the Zr_2Cu packing modified C/C-SiC-ZrC composites, labeled as ZrCu-CSiZr.

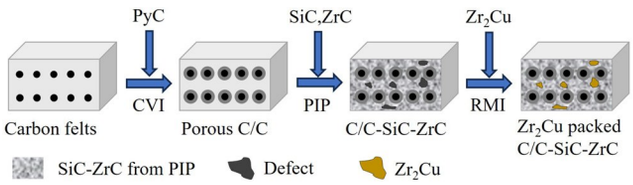

Fig.1 Schematic diagram of preparation procedure of ZrCu-CSiZr composites

The density and open porosity of the samples were measured using the Archimedes method. The mechanical properties were evaluated by a three-point bending test at a loading rate of 0.5 mm/min. The span was 20 mm. A minimum of five samples with dimensions of 30 mm×4 mm ×3 mm was tested. The ablation resistance of the samples was evaluated using 35 kW plasma equipment (Metco 9M). The plasma gun tip with 8 mm in internal diameter was extended by 60 mm from the sample. Samples with dimensions of 12 mm×12 mm×12 mm were placed perpendicularly in a flame for 20 s, and the surface temperature during ablation was monitored with an infrared thermometer. Linear and mass ablation rates were determined by the changes in thickness and mass before and after ablation, respectively.

Phase analysis of the composites was conducted by X-ray diffractometer (XRD, AXS D8 ADVANCE). The morphology and elemental composition of samples were examined using scanning electron microscope (SEM, MLA FEG 650) equipped with energy dispersive spectrometer (EDS, Oxford INCA).

3 Results and Discussion

3.1 Microstructure and composition

The bulk density and open porosity of CSiZr and ZrCu-CSiZr are summarized in Table 1. The bulk density of the composites increases from 1.91 g/cm^3 to 2.24 g/cm^3, while the

Table 1 Bulk density and open porosity of composites

Sample	Bulk density/g·cm^{-3}	Open porosity/%
CSiZr	1.91	18.10
ZrCu-CSiZr	2.24	13.15

open porosity decreases from 18.10% to 13.15%. This indicates that PIP C/C-SiC-ZrC composites can be densified quickly and efficiently by Zr_2Cu packing treatment.

Fig.2 shows the XRD patterns of the composites before and after the packing treatment. Initially, the raw composites contain C, ZrC, and SiC. However, in the XRD pattern of the ZrCu-CSiZr sample, ZrCu peaks are detected instead of Zr_2Cu, indicating incomplete consumption of zirconium due to its reaction with carbon to form ZrC during the Zr_2Cu melt impregnation process.

SEM images and EDS results of the composites are displayed in Fig. 3. Fig. 3a presents a representative microstructure of the CSiZr surface, revealing a considerable number of macropores. The cross-section (Fig. 3b) exhibits two main types of pores in CSiZr composites: external macropores (approximately hundreds of microns) between fiber bundles and a few micropores inside the fiber bundles (approximately 10 μm). The presence of these pores is attributed to volume shrinkage caused by gas molecules produced by the organic precursor during the pyrolysis process, making it difficult to achieve a dense ceramic matrix via the PIP process. This restriction is inherent in the preparation of CSiZr composites through PIP[34]. After packing, the composites are generally dense without apparent pores (Fig. 3c – 3d), indicating that the Zr_2Cu alloy used for infiltration has appropriate viscosity and good permeability, which can effectively fill the pores, improving the density of the CSiZr composites, as consistent with Table 1. The inset of Fig. 3d shows that the grey compact areas in spot 1 are ZrCu infiltration. To further investigate the matrix and infiltration, area A in Fig. 3c is enlarged, as shown in Fig. 3e, and corresponding element mappings are shown in Fig. 3f–3j. The bright white loose area is the PIP-impregnated SiC-ZrC matrix, while the light grey flat dense area corresponds to melt-infiltrated ZrCu. Notably, the micropores within the PIP SiC-ZrC matrix are unfilled due to the tiny size of these pores, and this issue may be potentially solved by further increasing the melt impregnation temperature.

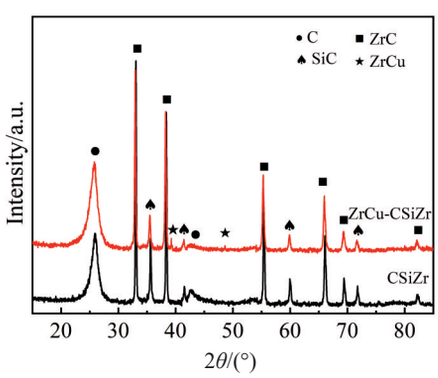

Fig.2 XRD patterns of composites

3.2 Mechanical property

The mechanical properties of the composites are listed in Table 2. Compared with CSiZr, which has a flexural strength of 122.78±8.09 MPa and a flexural modulus of 12.7±3.11 GPa, ZrCu-CSiZr exhibits superior mechanical properties, with a flexural strength of 135.53±5.40 MPa and a flexural modulus of 14.53±1.97 GPa. These improvements are attributed to ZrCu packing.

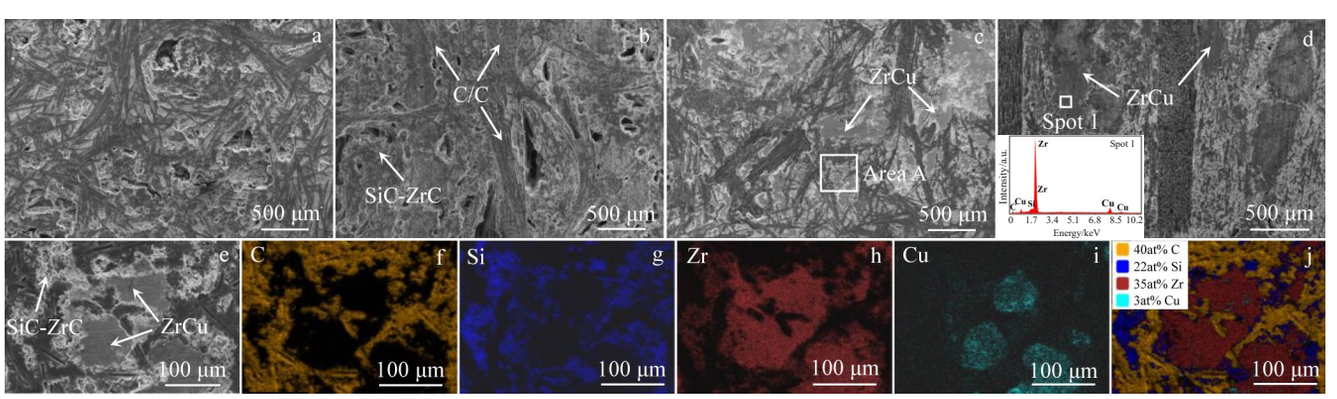

Fig.3 SEM images of surface (a, c) and cross-section (b, d) of composites CSiZr (a – b) and ZrCu-CSiZr (c – d); magnification of area A in Fig.3c (e); EDS element mappings corresponding to Fig.3e (f–j)

Table 2 Mechanical and ablation properties of the composites

Sample	Flexural strength/ MPa	Flexural modulus/ GPa	Linear ablation rate/ ×10^{-3} mm·s^{-1}	Mass ablation rate/ ×10^{-3} g·s^{-1}	Surface temperature/℃
CSiZr	122.78±8.09	12.7±3.11	4.32	3.09	1820
ZrCu-CSiZr	135.53±5.40	14.53±1.97	2.60	2.77	1750

Load-displacement curves of the composites, illustrating pseudoplastic fracture behavior, are shown in Fig. 4. As observed, ZrCu-CSiZr can withstand higher bending loads than CSiZr. During the initial stages of flexural loading, the loads applied to both composites increase linearly with displacement, exhibiting elastic deformation behavior. As the load increases, the elastic deformation limits of the composites are reached, leading to deviations from the initial straight line and entry into the inelastic deformation stage, accompanied by a decrease in elastic modulus of the composites. With further increase in flexural load, CSiZr exhibits a zigzagging drop zone, demonstrating the toughening effect of the fibers in the flexure test (i.e., crack deflection, fiber bridging, and fiber pull-out). In contrast, ZrCu-CSiZr shows a more pronounced short sudden break, with damage closely related to the strength of the interface. This is due to the denser short-cut fiber layer post-Zr_2Cu impregnation, which increases load-bearing capacity and brittleness. In the later stages of the curve, a "stepped" decrease is observed due to toughening effects such as fiber bridging.

Fracture morphologies of the composites are displayed in Fig.5. According to Fig.5a and 5c, the fiber bundles in the non-woven layers of both composites are heavily pulled out. The non-woven layer of the carbon felts is composed of parallel fiber bundles, with slight pores between the individual fibers, allowing only a small amount of pyrolytic carbon to deposit on the fiber surface, and resulting in a weak fiber/matrix interface. During loading, cracks tend to spread along this interface, leading to significant bundle pull-out, and effectively absorbing energy. As shown in Fig. 3, ZrCu impregnation is almost absent in the non-woven layer, resulting in similar fracture morphologies for the two samples. However, the fracture morphologies of the short-cut fiber webs with ZrCu concentration differ significantly, as shown in Fig.5b and 5d. CSiZr exhibits a loose distribution of ceramics and winding cracks, indicating relatively low load-bearing capacity. Conversely, ZrCu-CSiZr displays a relatively compact inner matrix with sintered ZrCu, reducing the pore defects and bonding the PIP SiC-ZrC matrix tightly, which can create a strong combination between different phases in the ceramic matrix. Therefore, the composites acquire a more effective ability to resist external loads and to enhance the flexural strength.

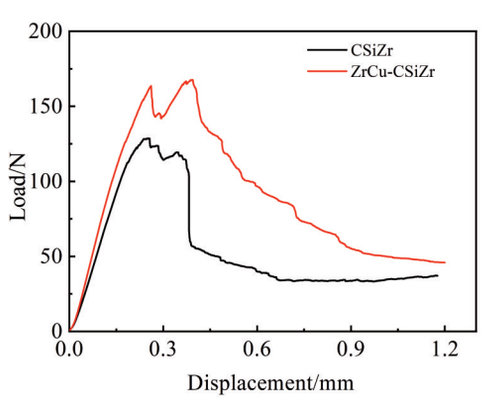

Fig.4 Load-displacement curves of composites

3.3 Ablation property

The composites were exposed to a plasma flame for ablation tests, as CSiZr composites are typically used to make high-temperature components. The ablative properties of the two composites are shown in Table 2. The linear ablation rate of ZrCu-CSiZr is 2.60×10^{-3} mm/s, which is 39.8% less than that of CSiZr. The mass ablation rates of CSiZr and ZrCu-CSiZr are 3.09×10^{-3} and 2.77×10^{-3} g/s, respectively. Notably, the maximum surface temperature of ZrCu-CSiZr is lower than that of CSiZr, indicating the evaporation of copper during ablation, which contributes to ablative resistance enhancement.

Fig.6 shows XRD patterns of the composites after ablation, revealing the presence of SiO_2 and ZrO_2, which are obtained by the oxidation of ZrC and SiC phases. No diffraction peaks containing any Cu phase are detected due to the low copper content and its evaporation during ablation.

SEM images and EDS results, presented in Fig. 7, provide further insights into the ablation behavior of the composites. The surface of ablated CSiZr exhibits a glassy oxide layer with cracks formed during cooling (Fig. 7a). In the magnified view (Fig. 7b), numerous particles are dispersed within the glassy coating. These particles act as pins and enhance the anti-erosion ability of the protective barriers. Analysis of Fig. 7c alongside Fig. 7g – 7h indicate that the bright white diffuse particles (1 – 5 μm) are identified as ZrO_2, and a dark continuous substance is SiO_2 film. Fig. 7d shows a protective layer of SiO_2-ZrO_2 based on XRD patterns (Fig. 6) and EDS results (Fig. 7i – 7j), which is formed on the ablated surface of ZrCu-CSiZr. The difference is that many small pores result from gas escaping during ablation (Fig. 7e). Notably, small pores in Fig. 7e resulted from gas escape during ablation. Importantly, nano-sized ZrO_2 particles are detected in the SiO_2 protective layer of ZrCu-CSiZr (Fig. 7f), attributed to the cooling effect of ZrCu during ablation[11,35], which enhances

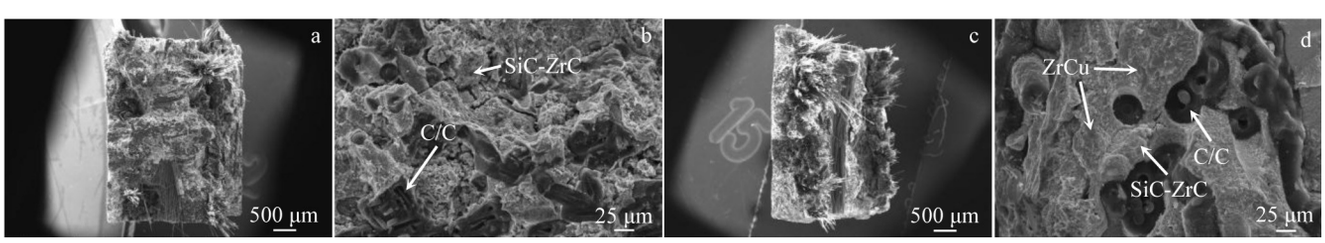

Fig.5 Fracture morphologies of composites: (a–b) CSiZr and (c–d) ZrCu-CSiZr

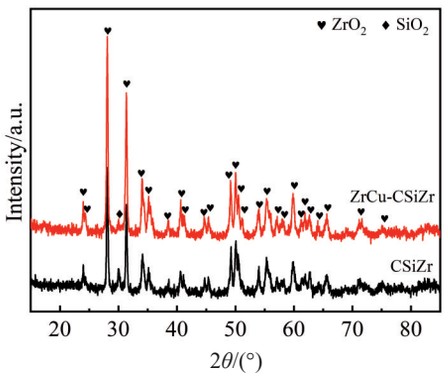

Fig.6 XRD patterns of composites after ablation

pinning effects and reduces SiO_2 consumption in ablative environment.

3.4 Ablation mechanism

When corroded by the plasma torch, the sample surfaces undergo heavy chemical erosion and mechanical denudation (flame scouring) [23,36]. The predominant reactions during the ablation process are as follows:

$$2C(s) + O_2(g) = 2CO(g) \quad (1)$$

$$C(s) + O_2(g) = CO_2(g) \quad (2)$$

$$ZrC(s) + \frac{3}{2}O_2(g) = ZrO_2(s) + CO(g) \quad (3)$$

$$ZrC(s) + 2O_2(g) = ZrO_2(s) + CO_2(g) \quad (4)$$

$$SiC(s) + \frac{3}{2}O_2(g) = SiO(g) + CO_2(g) \quad (5)$$

$$SiC(s) + 2O_2(g) = SiO_2(l) + CO_2(g) \quad (6)$$

$$4ZrCu(s) + 5O_2(g) = 2Cu_2O(s) + 4ZrO_2(s) \quad (7)$$

$$Cu_2O(s) = Cu_2O(l) = Cu_2O(g) \quad (8)$$

$$SiO_2(l) = SiO_2(g) \quad (9)$$

The ablation mechanism of the ZrCu-CSiZr sample is shown in Fig. 8. In the initial seconds of ablation, the plasma flame is in contact with the composite, causing a dramatic increase in surface temperature. The various phases in the ZrCu-CSiZr sample begin to oxidize. As previously observed[13], the Gibbs free energy of the oxidation of ZrC and SiC is lower in an oxygen-enriched environment, leading to preferential oxidation to form ZrO_2 and SiO_2. Meanwhile, ZrCu also oxidizes. According to Ref. [37], CuO is converted to Cu_2O at about 1120 °C. The oxidation products of ZrCu are presumed to be ZrO_2 and Cu_2O, as shown in Eq. (7). As ablation proceeds, the surface temperature of the sample rises, causing SiO_2 to melt and to form a molten film covering the composite surface. This film resists the erosion of the internal material by external airflow to a certain extent. However, the viscosity of the SiO_2 melt is low, making it susceptible to being washed away by the ablating flow, which increases the ablation rate. Fortunately, ZrO_2, with a higher melting point,

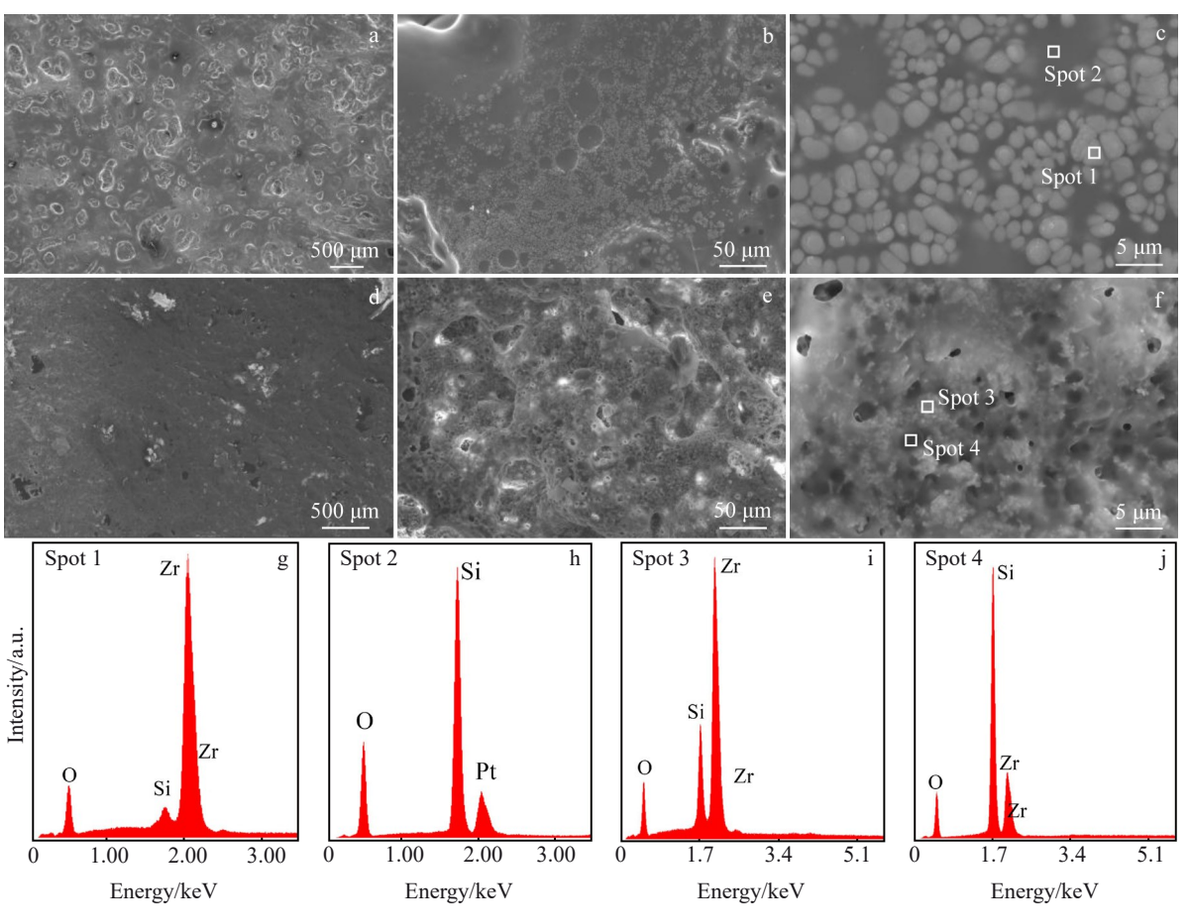

Fig.7 SEM images (a–f) and EDS results (g–j) of composites after ablation: (a–c) CSiZr; (d–f) ZrCu-CSiZr

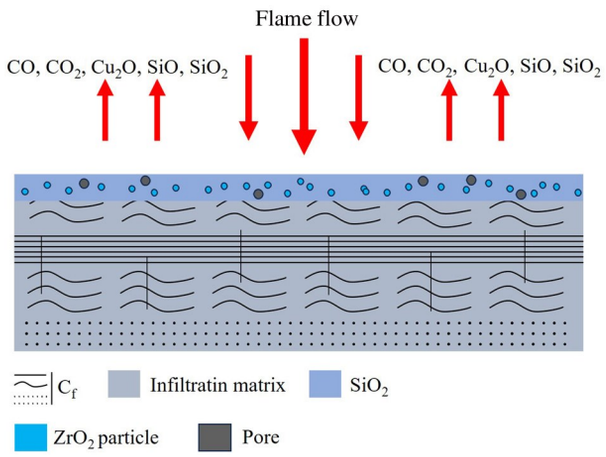

Fig.8 Schematic diagram of ZrCu-CSiZr during ablation

does not melt at the current temperature. It remains as particles embedded in the molten SiO_2 film, enhancing the stability of SiO_2 and effectively alleviating the consumption of the molten layer in high-temperature airflow. The gaseous products of these reactions, such as CO, CO_2, and SiO, will escape, causing micropores to form on the ZrO_2-fixed molten SiO_2. Cu_2O liquefies at about 1235 °C and evaporates when the temperature exceeds its boiling point (1800 °C), increasing the number of micropores. Significantly, the heat absorbed by the plasma flame through the evaporation of Cu_2O reduces the surface temperature, inhibiting the growth of ZrO_2 particles at a lower temperature. This makes the pinning effect more effective, providing adequate protection for the ZrCu-CSiZr composites.

4 Conclusions

1) The Zr_2Cu melt exhibits favorable wettability with the PIP C/C-SiC-ZrC matrix and efficiently fills the macropores, contributing to densification of the composites and a reduction in open porosity of 27.35%.

2) The flexural strength of Zr_2Cu packed C/C-SiC-ZrC composites is improved from 122.78±8.09 MPa to 135.53±5.40 MPa because the denser matrix provides greater resistance to external forces.

3) The ablation properties are enhanced, with mass loss rate and linear recession rate of 2.77×10^{-3} g/s and 2.60×10^{-3} mm/s after plasma ablation for 20 s, respectively. Excellent ablative properties are attributed to stronger pinning of fine nano-sized ZrO_2 in the SiO_2 molten protective layer and the volatilization of the Cu-containing phase.

References

1 Pan Suyan, Zhong Zhihong, Song Kuijing *et al. Rare Metal Materials and Engineering*[J], 2024, 53(8): 2232 (in Chinese)

2 Weng Yuanqi, Yang Xin, Chen Feixiong *et al. Journal of the European Ceramic Society*[J], 2023, 43(11): 4602

3 Wang Fuqiang, Chen Jian, Wang Kunjie *et al. Rare Metal Materials and Engineering*[J], 2022, 51(3): 873

4 Jin Xiaochao, Fan Xueling, Lu Chunsheng *et al. Journal of the European Ceramic Society*[J], 2018, 38(1): 1

5 Li Zhaoqian, Li Hejun, Zhang Shouyang *et al. Ceramics International*[J], 2013, 39(7): 8173

6 Wu Huang, Yi Maozhong, Ge Yicheng *et al. Materials Characterization*[J], 2018, 138: 238

7 Yao Xiyuan, Chen Miaomiao, Feng Guanghui. *Rare Metal Materials and Engineering*[J], 2020, 49(1): 241 (in Chinese)

8 Arai Yutaro, Inoue Ryo, Goto Ken *et al. Ceramics International*[J], 2019, 45(12): 14481

9 Wang Hui, Ding Chenshi, Xie Zhuoming *et al. Rare Metal Materials and Engineering*[J], 2024, 53(5): 1321

10 Fu Yu, Chen Meiru, Xiao Peng *et al. Ceramics International*[J], 2023, 49(18): 29391

11 Shao Yuxuan, Yang Yong, Wang Yonggang *et al. Surface and Coatings Technology*[J], 2023, 459: 129387

12 Dai Jixiang, Sha Jianjun, Wang Yongchang *et al. Rare Metal Materials and Engineering*[J], 2016, 45(3): 742

13 Weng Yuanqi, Yang Xin, Chen Feixiong *et al. Ceramics International*[J], 2022, 48(6): 7937

14 Wu Huang, Yi Maozhong, Ge Yicheng *et al. Materials Characterization*[J], 2018, 138: 238

15 Zhu Yulin, Wang Song, Chen Hongmei *et al. Ceramics International*[J], 2014, 40(2): 2793

16 Peng Zheng, Miao Chunmao, Sun Wei *et al. Transactions of Nonferrous Metals Society of China*[J], 2022, 32(10): 3349

17 Zhao Zhigang, Li Kezhi, Li Wei. *Corrosion Science*[J], 2021, 189: 109598

18 Liu Rongjun, Liu Xingyu, Wang Yanfei *et al. Ceramics International*[J], 2021, 47(16): 23610

19 Li Jun, Yang Xin, Su Zhean *et al. Transactions of Nonferrous Metals Society of China*[J], 2016, 26(10): 2653

20 Li Kezhi, Xie Jing, Fu Qiangang *et al. Carbon*[J], 2013, 57: 161

21 Yang Xiaohui, Li Kezhi, Bai Longteng *et al. Vacuum*[J], 2018, 156: 334

22 Tan Wenlong, Li Kezhi, Li Hejun *et al. Vacuum*[J], 2015, 116: 124

23 Jiao Xiaoyang, He Qinchuan, Tan Qing *et al. Journal of the European Ceramic Society*[J], 2023, 43(14): 5851

24 Li Kezhi, Xie Jing, Li Hejun *et al. Journal of Materials Science and Technology*[J], 2015, 31(1): 77

25 Yan Chunlei, Liu Rongjun, Cao Yingbin *et al. Ceramics International*[J], 2014, 40(7): 10961

26 Zhu Shibu, Meng Xiangli, Zhang Qiang *et al. Equipment Environmental Engineering*[J], 2019, 16(10): 32

27 Zhao Zhigang, Li Kezhi, Liu Qing *et al. Vacuum*[J], 2018, 156: 123

28 Liu Chunxuan, Su Zhean, Huang Qizhong *et al. Journal of Alloys and Compounds*[J], 2014, 597: 236

29 Kong Yingjie, Yu Xinmin, Pei Yuchen. *Equipment Environmental Engineering*[J], 2016, 13(3): 88

30 Zhao Zhigang, Li Kezhi, Li Wei *et al. Corrosion Science*[J], 2021, 181: 109202
31 Li Hongtao, Yang Xin, Chen Feixiong *et al. Ceramics International*[J], 2023, 49(8): 12173
32 Liu Lei, Li Hejun, Shi Xiaohong *et al. Solid State Sciences*[J], 2013, 25: 78
33 Yu Hang, Li Kezhi, Lu Jinhua *et al. Corrosion Science*[J], 2024, 227: 111732
34 Xie Jing, Jia Yujun, Zhao Zhigang *et al. Vacuum*[J], 2018, 157: 324
35 Cheng Yehong, Zhang Fan, Ma Denghao *et al. International Journal of Applied Ceramic Technology*[J], 2022, 20(3): 1636
36 Shao Mengmeng, Chen Zhaoke, Wang Xinshuang *et al. Transactions of Nonferrous Metals Society of China*[J], 2023, 33(1): 220
37 Weng Yuanqi, Yang Xin, Chen Feixiong *et al. Corrosion Science*[J], 2022, 209: 110801

Zr_2Cu封填改性对PIP制备的C/C-SiC-ZrC复合材料微观结构和力学及烧蚀性能的影响

解　静[1]，张　前[1]，任　静[1]，苏海龙[2]，田录录[2]，支雄辉[2]，孙国栋[1]，李　辉[1]，王　龙[3]
(1. 长安大学 材料科学与工程学院，陕西 西安 710061)
(2. 西安鑫垚陶瓷复合材料股份有限公司，陕西 西安 710089)
(3. 火箭军工程大学 智剑实验室，陕西 西安 710025)

摘　要：为了改善聚合物浸渍裂解法（PIP）制备的C/C-SiC-ZrC复合材料的致密度和性能，以Zr_2Cu为填料，采用低温反应熔体浸渍工艺（RMI）对复合材料进行封孔，研究了Zr_2Cu封填后复合材料的微观结构、力学性能和烧蚀性能。结果表明：在Zr_2Cu浸渍过程中，熔体有效地填充了复合材料的大孔隙，并且由于部分锆与碳发生化学反应，Zr_2Cu转化为ZrCu。材料的密度从1.91 g/cm^{3}增加至2.24 g/cm^3，孔隙率降低了27.35%。此外，封填后的C/C-SiC-ZrC复合材料的抗弯曲强度从122.78±8.09 MPa提高至135.53±5.40 MPa，等离子体烧蚀20 s后，与PIP C/C-SiC-ZrC相比，表现出更优越的耐烧蚀性，其质量烧蚀率和线性烧蚀率分别为2.77×10^{-3} g/s和2.60×10^{-3} mm/s。低熔点含铜相的“自蒸发”效应吸收了等离子火焰的热量，进一步降低了烧蚀温度，促进了SiO_2熔化层内细化ZrO_2颗粒的形成，这为Zr_2Cu封填C/C-SiC-ZrC复合材料提供了更稳定的侵蚀保护。

关键词：C/C-SiC-ZrC复合材料；Zr_2Cu封填；微观结构；力学性能；烧蚀性能

作者简介：解　静，女，1986年生，博士，副教授，长安大学材料科学与工程学院，陕西 西安 710061，E-mail：xiejing@chd.edu.cn